Modeling fume formation and deposition in kraft recovery boilers

JORMA K. JOKINIEMI, JOUNI PYYKÖNEN, PIRITA MIKKANEN, AND ESKO I. KAUPPINEN

ABSTRACT

The ABC mathematical model of fume formation is based on aerosol dynamics. The model takes into account the mechanisms of gas-phase chemical reactions, homogeneous and heterogeneous condensation, agglomeration, and deposition. Researchers can use the model to estimate the size distributions and deposition rates of fume particles and vapors in a kraft recovery boiler. Model results are compared with fume measurements made in an operating recovery boiler in a mill.

Application:

The computer simulation can help to solve deposition problems in kraft recovery boilers.

KRAFT RECOVERY BOILERS LOSE efficiency in convective heat transfer as a result of slagging and fouling. Deposits from carryover and fumes lead to plugging between the tubes of heat exchangers, which impedes the flow of hot gas. Fume deposition depends on the vapor-phase reactions, particle size, and chemical composition, and on the boiler geometry, flow fields, temperature distributions, and heat transfer phenomena.

We have constructed a general aerosol computer model named "ABC" as an acronym for "aerosol behavior in combustion" *(1)*. This model takes into account fume particle formation and growth, fume particle deposition, and the chemistry of sodium, potassium, and chloride species. As an example case, we have calculated fume deposition in a boiler on which we have carried out detailed studies in characterizing fume particles *(2–5)*.

The ABC model improves our ability to predict the formation, growth, and chemical composition of deposits that cause slagging and fouling. It also makes it possible for us to analyze the dependence of deposition formation on boiler temperatures and geometry, flow conditions, and the volatilization of sodium, potassium, and chloride species.

AEROSOL DYNAMICS

Generally, 100 µm is considered the maximum size of an aerosol particle. Aerosol particles form and increase in size through the condensation of alkali species vaporized in the furnace. Condensation can be homogeneous or heterogeneous. The principles of aerosol dynamics cover the gas-phase reactions of the vaporized species, their condensation to form and grow particles, the agglomeration of particles, and the deposition of particles and vapor.

Homogeneous condensation

In the furnace, volatilized sodium and potassium vapors can become supersaturated as a result of flue gas cooling or chemical reactions. The saturation ratio of a vapor is defined as the ratio of its partial pressure to its equilibrium pressure. If the saturation ratio is larger than 1.0, the vapor is supersaturated.

For example, NaOH reacts with SO_2 to form Na_2SO_4(g). Gaseous sodium sulfate has a low equilibrium vapor pressure, so this vapor becomes supersaturated immediately after it forms. Thermodynamically, supersaturation is not a favored state, and the vapor starts to condense. Condensation allows the partial vapor pressure to decrease toward its equilibrium value.

At a supersaturation much higher than the ratio of 1.0, a process called "homogeneous nucleation" occurs. Vapor molecules stick together and form new aerosol particles, provided there are no other particles in the flue gas. At this critical supersaturation, tiny aerosol particles are formed at a rate that can be predicted according to the principles of thermodynamics and kinetics *(6)*.

Heterogeneous condensation

The gas may already contain particles, however, such as metal oxide seed particles. Vapor starts to condense on the surface of these particles before any new particles can be formed by homogeneous nucleation.

Condensation on surfaces starts at lower supersaturation ratios than the ratio at which homogeneous nucleation begins. The particles grow at a rate that can be determined by solving the heat and mass transfer equations for single particles.

Agglomeration

In agglomeration, particles collide with each other and stick together. The collision rate is determined by Brownian movement and turbulent diffusion. When submicron particles collide, they always stick together.

Particle size, chemical composition, and process conditions determine the properties of these agglomerated particles. If the colliding particles are liquid, they form a new spherical liquid droplet. Colliding solid particles stay together by Van der Waals attraction. Agglomerates formed in black liquor combustion tend to sinter together and form particles with a complex morphology.

MODELING AEROSOL DYNAMICS IN THE ABC CODE

In the ABC code, we simulate a combustion process. As input data, we use both the rates at which the elements involved are vaporized and the possible particle size for the initial seed. The changes in the particle size and chemical composition arise from chemical reactions, homogeneous nucleation, vapor condensation, agglomeration, and deposition. The whole process is described by the general dynamic equation *(6)*.

We assume that the combustion process is in a condition of steady state. Thus, we solve the aerosol general dynamic equation in one-dimensional, stationary form along the flow direction. The mass size distribution of a species can be calculated by solving the condensed-phase general dynamic equation, where the particle size spectrum is divided into a number of grid points:

See page 181 for equation 1

Here, r_{dk} is the average particle density, and Y_{jk} is the mass fraction of species j at the kth grid point corresponding to radius r_k. The first term on the right, denoted "gtp" in subscript, corresponds to the particle formation of homogeneous nucleation and growth by condensation and chemical reactions. The second term, denoted "agg", describes agglomeration.

The third term pertains to the rate of particle removal resulting from deposition on boundary surfaces. V_{dk} is the particle deposition velocity, A_d is the deposition area, and ΔV is the axial volume step. The particle velocity, u, is calculated by taking into account gas velocity, Stokes drag, and gravitation.

The rate of change in the molar concentration of a gas-phase species is given by the following equation:

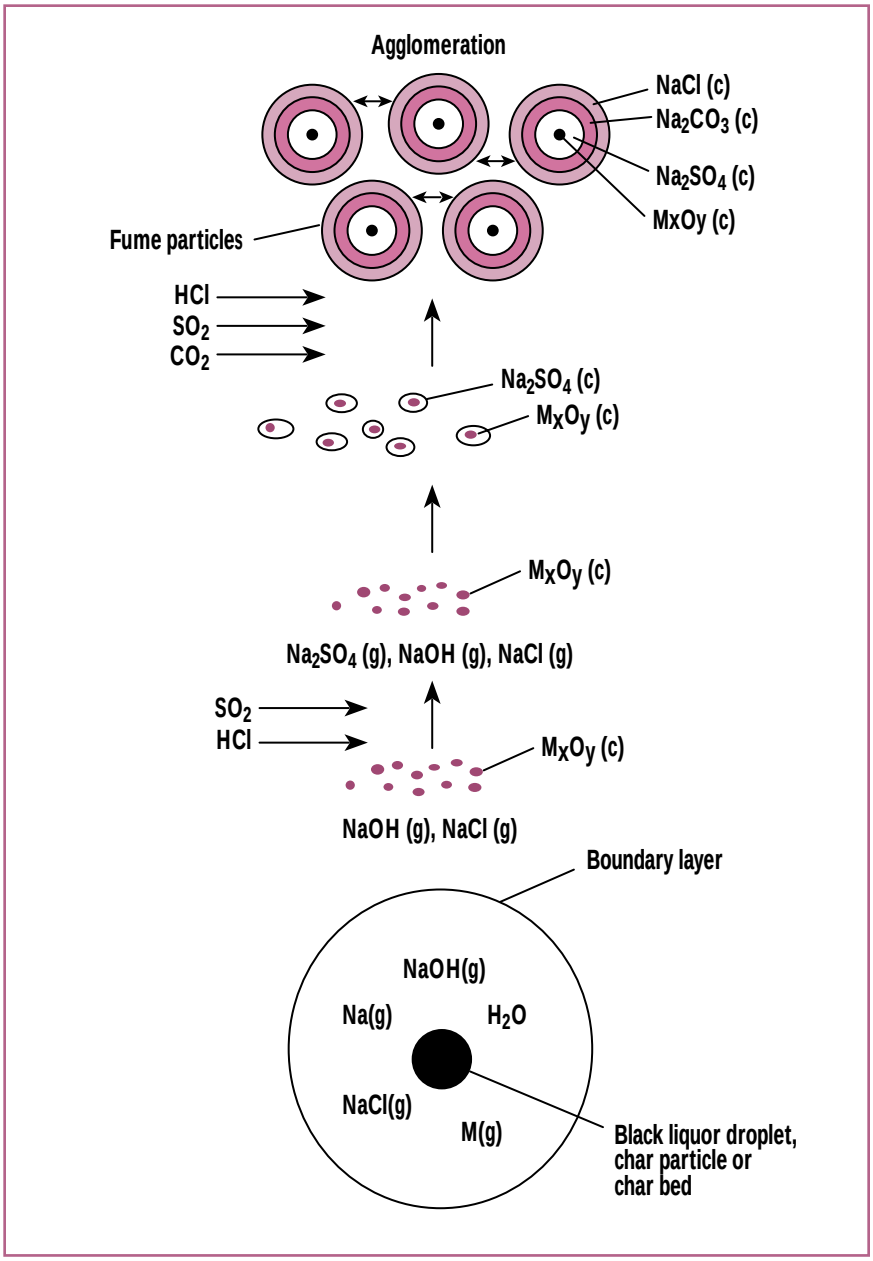

1. The scheme of sodium fume formation in the kraft recovery boiler in the presence of metal oxide seeds (M = metal, M_xO_y = metal oxide, g = gas, c = condensed).

See page 181 for equation 2

where c_j is the gas-phase molar concentration of species j. The first term on the right, indicated by "form", represents the formation rate of these species. The formation rate can be calculated from the local gas-phase chemical equilibrium or from reaction kinetics. The second term, "gtp", describes the vapor depletion rate by nucleation, condensation, and chemical reactions.

The third term represents the depletion rate arising from vapor deposition by condensation and chemical reactions on structures. V_v is the vapor deposition velocity, and A_d is the deposition area. Here, time is related to the axial position by the

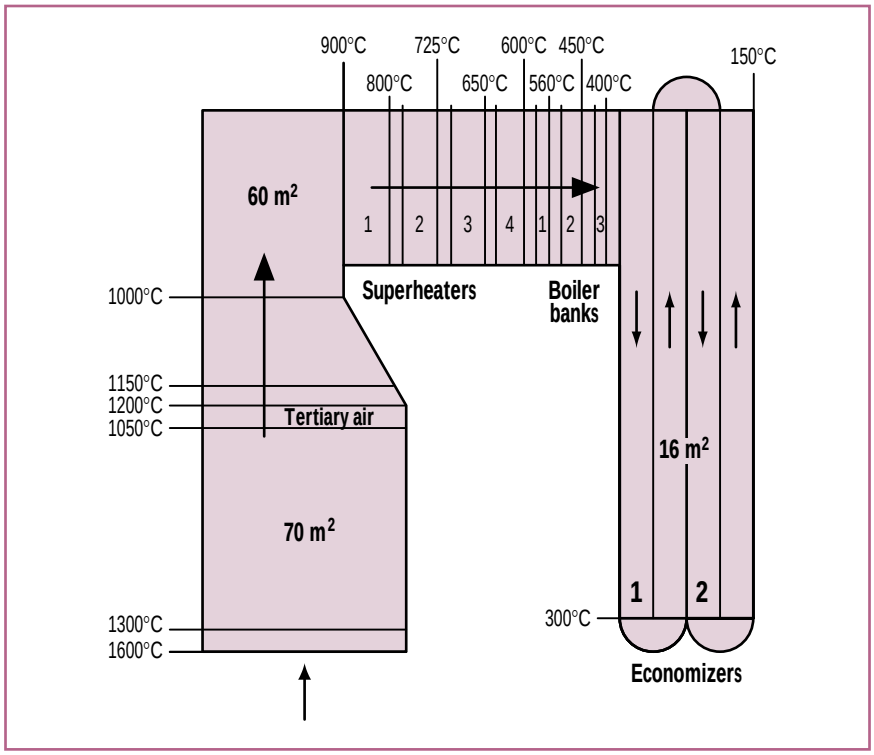

2. Layout of the simulated boiler, showing gas temperatures and cross-sectional areas.

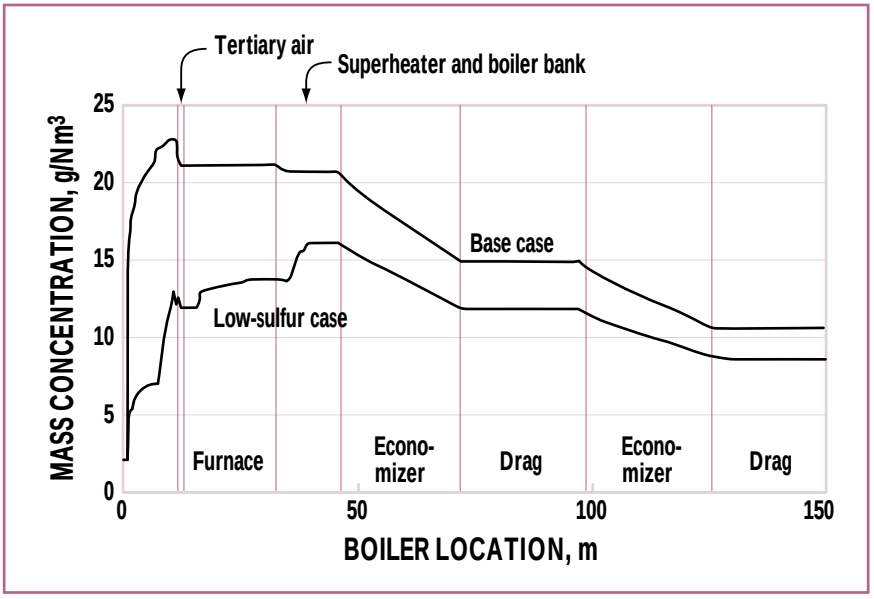

3. For the low-sulfur case, increases in the concentration of fume particles indicate three steps in the chemistry of particle formation.

gas velocity (u_g). A more detailed description of the ABC model can be found elsewhere *(1)*.

FUME FORMATION

Release

In the kraft recovery boiler, fractions of the black liquor contents are released into the gas phase, including Na, S, Cl, C, and K. The release mechanisms of these elements are not known in detail yet. However, the following mechanisms are possible:

- Release during the pyrolysis and char-burning stages before the black liquor droplets reach the char bed
- Release at the char bed
- Release from carryover particles during pyrolysis and char burning.

Based on recent results from laboratory experiments *(7)*, one mechanism that does not seem important is the release of Na vapors during pyrolysis of the black liquor droplets. According to equilibrium calculations *(8)*, the release at the char bed is less significant than the release from carryover particles during pyrolysis and char burning, even at the expected maximum bed temperature *(9)*.

The volatilization mechanism is important if one wants to predict the dependence of volatilization on black liquor properties. In the ABC model, however, we take the elemental volatilization fractions from boiler mass balance measurements and start the simulation above the char bed with the given extents of release. The actual release mechanism is not involved in our calculations of fume particle formation.

Gas-phase reactions

In the gas phase, Na, K, NaCl, and KCl simultaneously mix and react with gaseous H_2O, CO_2, CO, O_2, H_2S, SO_2, OH, and HCl to form NaOH, KOH, NaCl, KCl, Na_2SO_4, and K_2SO_4. The following gas-phase reactions dominate Na behavior at high temperatures:

$$Na^+ + H_2O\ [\rightarrow]\ NaOH + H^+ \quad (3)$$

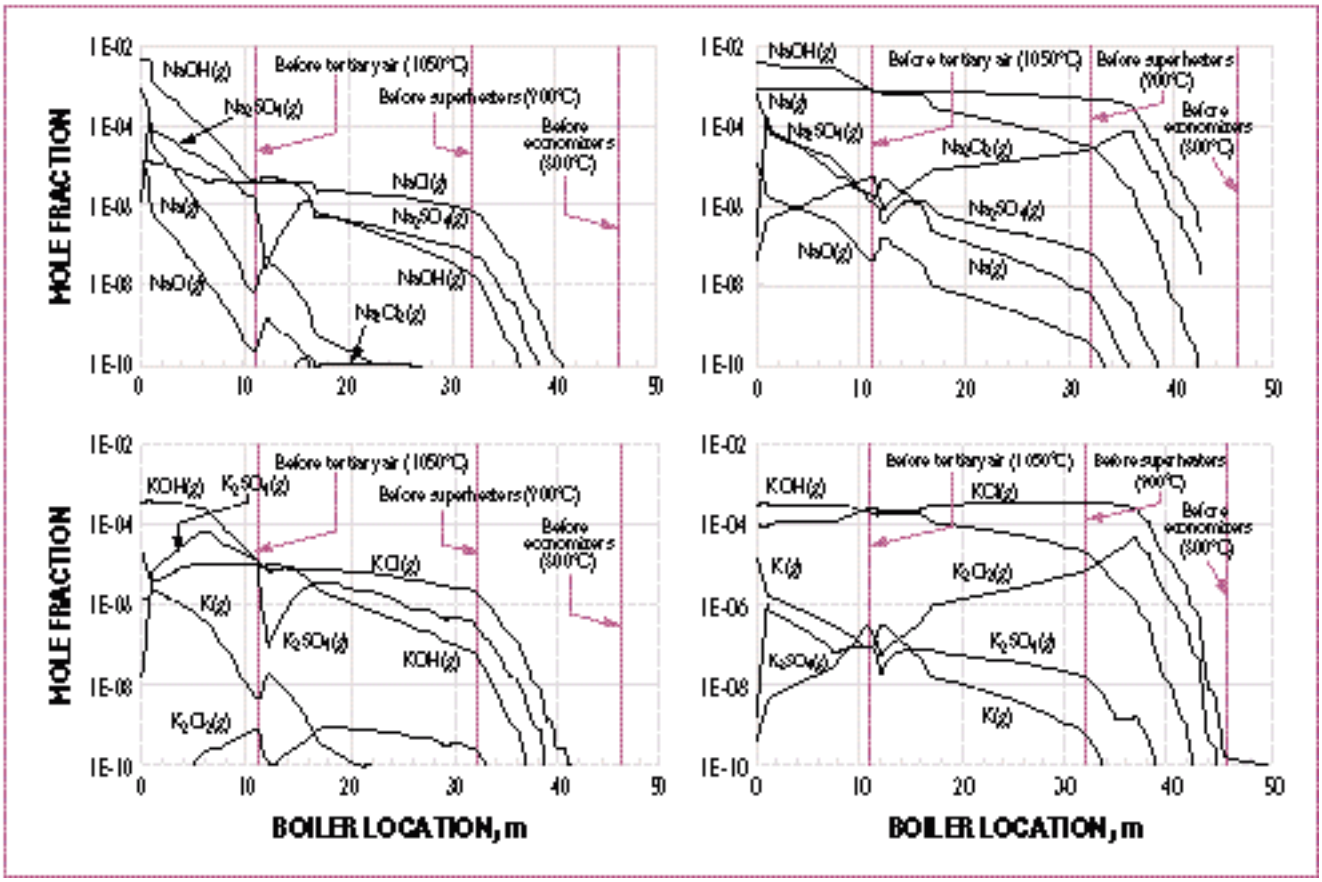

4. Composition of the gas with respect to sodium and potassium for the base case and the low-sulfur case.

$$NaOH + HCl \; [\rightarrow] \; NaCl + H_2O \quad (4)$$

The reactions for K are similar. The formation of alkali hydroxides and chlorides is rapid. Calculations with detailed chemical kinetics *(10, 11)* show that equilibrium is reached in a few milliseconds.

Fume formation mechanisms

Fume formation depends on the gas temperature in the furnace. At high temperatures of 1400–1600°C *(9, 12)*, the volatilized Na and K convert rapidly to hydroxides and chlorides in the gas phase. According to equilibrium calculations, alkali hydroxides and chlorides convert to sulfates by reactions with SO_2 as the temperature decreases.

$$2NaOH(g) + SO_2(g) + 1/2O_2 \; [\rightarrow] \; Na_2SO_4(g,c) + H_2O(g) \quad (5)$$

$$2NaCl(g) + SO_2(g) + 1/2O_2 + H_2O(g) \; [\rightarrow] \; Na_2SO_4(g,c) + 2HCl(g) \quad (6)$$

Element	DRY SOLIDS CONTENT, % by wt. Base case	DRY SOLIDS CONTENT, % by wt. Low sulfur	VOLATILIZED FRACTION, % Base case	VOLATILIZED FRACTION, % Low sulfur
Na	19.9	20.6	10	10
K	2.6	2.7	10	10
Cl	0.18	1.3	5	50
S	6.4	2.6	35	15
C	30.0	30.8	97.5	97.5
N	0.15	0.15	100	100
O	37.0	0.15	100	100
H	3.0	3.3	100	100
Mech.*	0.78	0.80	…	…
Seeds	0.016	0.016	…	…

*Mechanically produced particles.

I. Fuel composition and volatilized fractions

There should be enough air for SO_2 formation because oxidizing

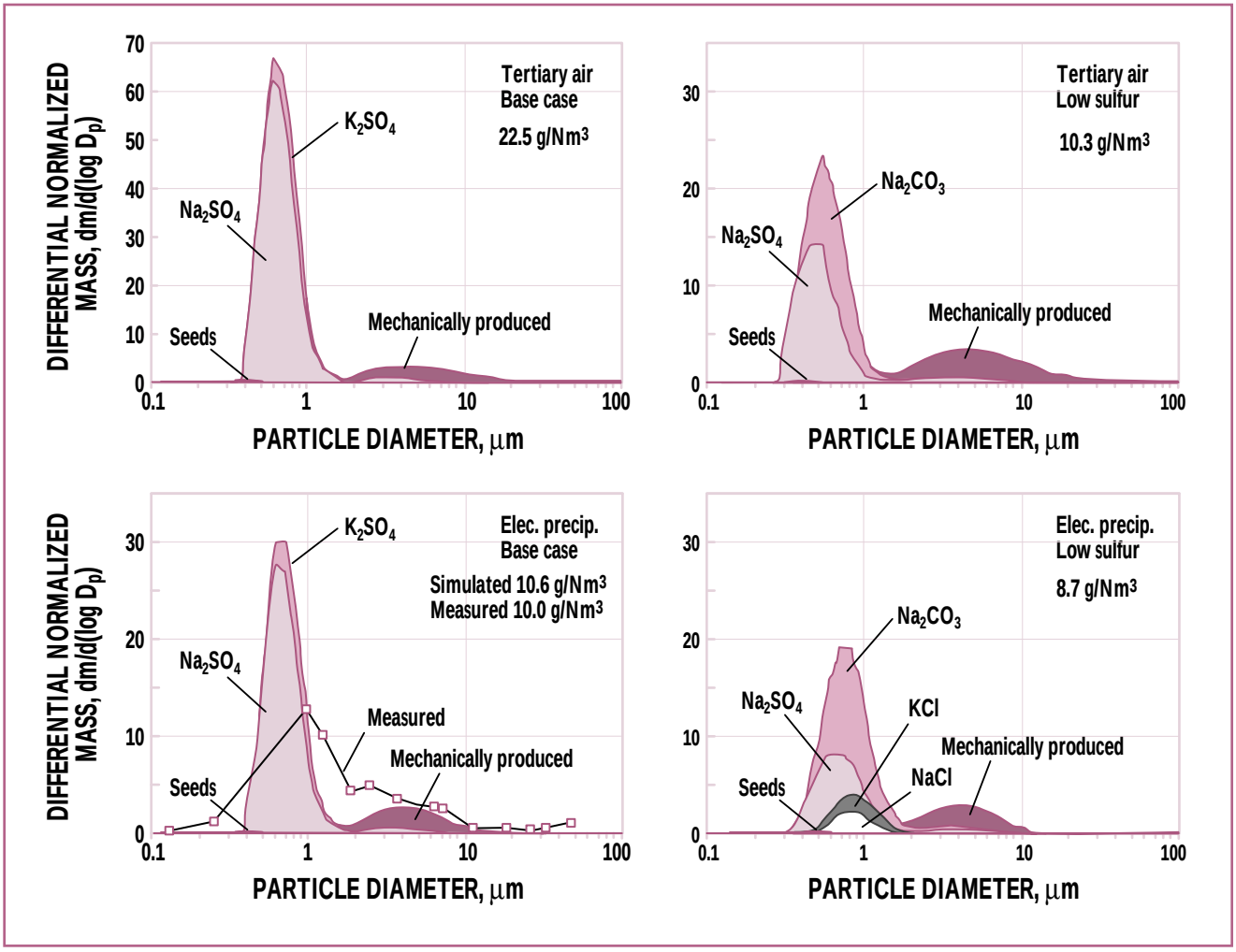

5. Particle mass size distribution before the injection of tertiary air for the base case (left) and the low-sulfur case (right) and before the electrostatic precipitator for each case. For the base case, the measured mass size distribution is also shown (lower left).

conditions prevail in the furnace *(9)*. If the maximum temperature is below 1400°C, sulfates form after the released alkali hydroxides and chlorides are mixed with the main gas components.

The formation of Na_2SO_4 in the gas phase can be limited as a result of kinetics *(11)*. However, recent results from laminar flow reactor experiments *(2)* and SEM samples taken from the upper furnace indicate that $Na_2SO_4(c)$ fume particles (condensed) have formed at temperatures above 1100°C. These indications mean that homogeneous or heterogeneous formation of $Na_2SO_4(c)$ fume can occur at high temperatures. The maximum temperature in the furnace is above the decomposition limit for $Na_2CO_3(c)$. Based on this thermodynamic consideration and on laminar flow reactor experiments and field measurements, we can conclude that $Na_2SO_4(c)$ instead of $Na_2CO_3(c)$ is the first alkali species to condense in the recovery boiler furnace. This conclusion contradicts the findings of earlier studies.

Because gaseous sodium and potassium sulfates have low equilibrium vapor pressures, these sulfates condense rapidly after they form. There are three possible ways for sodium sulfate fume particles to form initially in the furnace. They can:

1. Condense homogeneously (nucleation)
2. Condense directly on metal oxide seed particles
3. Form by surface reactions on metal oxide seed particles.

In the combustion of pulverized coal, tiny metal oxide seed particles are formed, even if only a fraction of

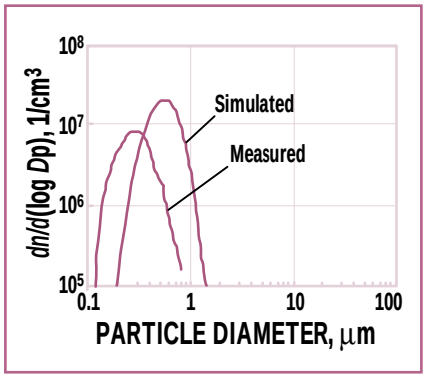

6. Number size distributions for the measured base case and simulated base case before the electrostatic precipitator.

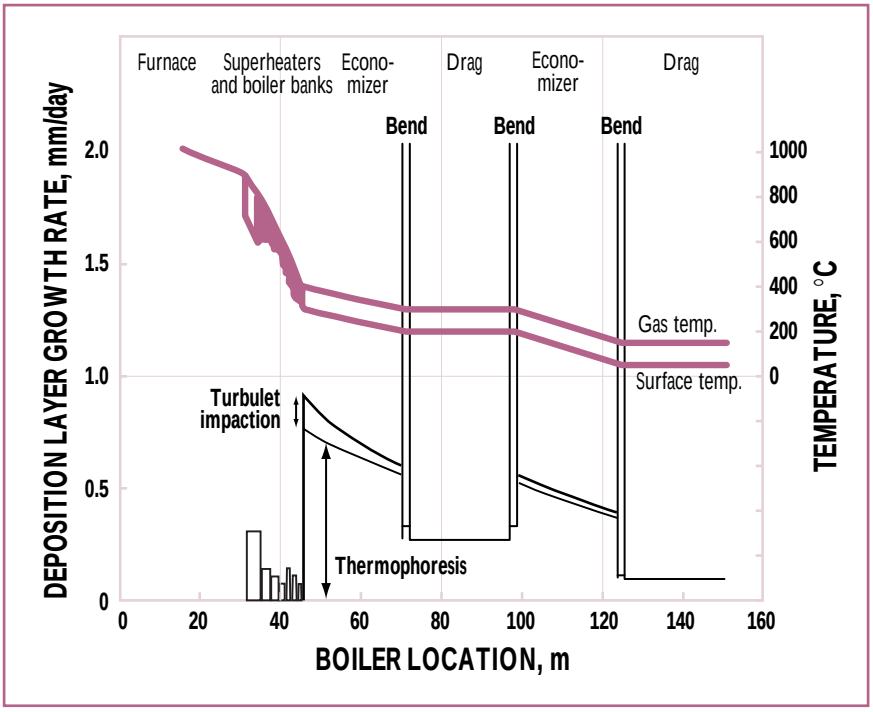

7. Growth rate of fume deposition as a function of boiler location and different deposition mechanisms in the base case. Temperatures are also shown for gas and heat exchanger surfaces.

the metals in coal are volatilized *(13)*. We have found metal oxides (such as MgO, SiO_2, CaO, and Fe_2O_3) in aerosol samples from kraft recovery boilers. The fraction of these metals is lower in black liquor than in coal. Nevertheless, based on ABC calculations with and without seeds and on our experience from aerosol formation in different combustion processes, we believe the initial mechanism to be heterogeneous (that is, the second or third possibility listed). According to equilibrium calculations, both homogeneous and heterogeneous sulfation reactions take place at the same temperature, which in our example calculation is about 1370°C.

When there is not enough SO_2 to bind all Na and K, these species convert to carbonates by surface reaction.

$$2NaOH(g) + CO_2(g) [\rightarrow] 2NaOH(c) + CO_2(g) [\rightarrow] Na_2CO_3(c) + H_2O(g) \quad (7)$$

Some of the chlorides condense directly as the temperature decreases.

$$NaCl(g) [\rightarrow] NaCl(c) \quad (8)$$

This improvement also explains the observation that low SO_2 levels are accompanied by low HCl levels, because the extra sodium binds chlorine and carbon. Alkali carbonates and sulfides are not stable in the gas phase, and surface reactions and/or condensation are necessary if these species are to form. Sulfides, however, should not form, because of the oxidizing conditions in the furnace. The fume formation mechanisms are illustrated in Fig. 1.

ABC DEPOSITION MODEL

Boundary layer theory for particle transport

The flow field in the boundary layer is divided into three regions:

1. Fully turbulent region
2. Buffer layer
3. Laminar sublayer.

In the fully turbulent region, which is furthest from the wall, the particle concentration is constant, in terms of being unaffected by the wall. In the buffer layer, the particle flux toward the wall surface is determined by particle turbulent diffusion *(14)*. In the laminar sublayer, which is closest to the wall, turbulent diffusion is assumed to decay in a cubic fashion, and additional mechanisms are needed to complete the deposition of particles.

For submicron particle deposition over the laminar sublayer, the mechanisms are thermophoresis and Brownian diffusion. Thermophoresis is a force experienced by particles when there is a temperature gradient in the gas. It is a result of greater momentum transfer from the gas molecules on the hot side of the particles compared with the cold side. For supermicron particles, the mechanisms are turbulent eddy impaction (flow parallel with the wall surface), inertial impaction (flow perpendicular to an obstacle), and gravitational settling.

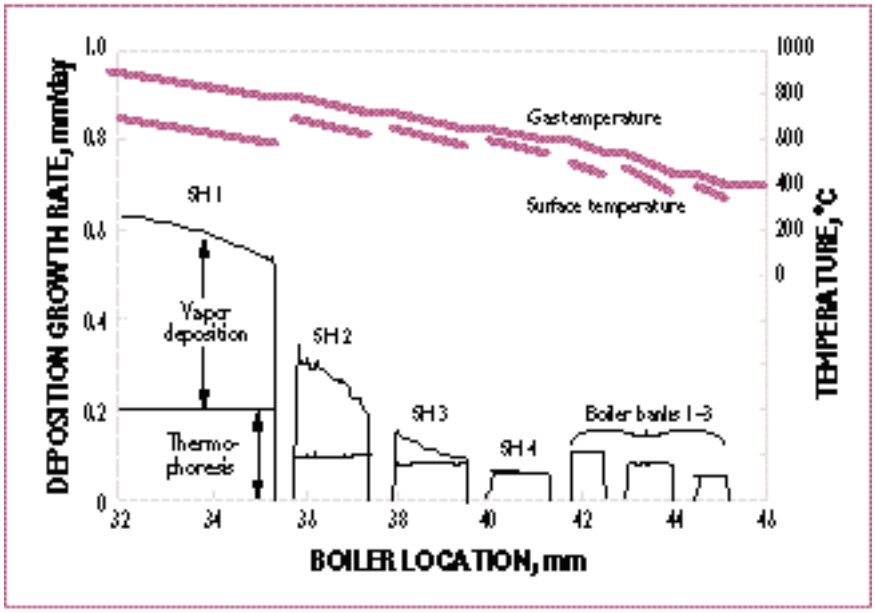

8. Fume deposition rate in the superheater and boiler bank section in the case of low sulfur.

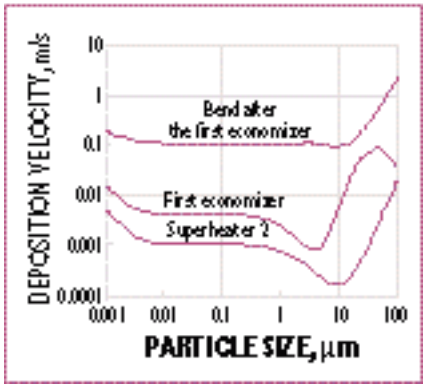

9. Deposition velocities as a function of particle size at different locations.

The total effective deposition velocity, V_d, in flows parallel with surfaces is *(15)*:

See page 181 for equation 9

where v_f is the turbulent diffusion velocity resulting from particle turbulent diffusion in the buffer layer, v is the deposition velocity in the laminar sublayer, J_p is the particle flux toward the wall surface, and $n(x)$ is the particle concentration in the fully turbulent region. The deposition velocity in the laminar sublayer depends on turbulence, thermophoresis *(16)*, diffusion, and impaction *(17)*.

For flows perpendicular to heat transfer tubes, the effective deposition velocity for supermicron particles is:

$$V_d = [h]u/\pi \qquad (10)$$

where [h] is the collection efficiency *(18)*.

All particles that reach the surface do not necessarily stick. Solid, supermicron particles may bounce back into the gas stream. The sticking efficiency is a function of particle size, density, and viscosity. The exact sticking efficiency is not usually known and must be determined experimentally.

Vapor deposition on heat exchanger surfaces

Vapors may deposit by direct condensation or by chemical reactions with surfaces. The ABC model includes diffusion through the boundary layer, chemical reactions, and diffusion through the reacted ash layer *(19)*. A more comprehensive description of the ABC deposition model is presented elsewhere *(20)*.

RECOVERY BOILER CALCULATIONS

The capabilities of the ABC model have been demonstrated in calculations for two kraft recovery boilers. The purpose was to predict alkali salt deposition on heat exchanger surfaces based on fuel composition, combustion conditions, and flow conditions. Here, we report the results from only one boiler because we found no substantial differences in aerosol behavior between the two. These results are the first results reported from recovery boiler simulations with the ABC model.

We already had a good set of data to validate the simulated results by virtue of detailed fume particle characterization studies that we had carried out on different boilers *(2–5)*. The studies included measurements to obtain the physical and chemical characteristics of aerosol particles, combined with gas composition and fuel data.

The particle number size distributions were measured in the Stokesian size range of 0.02–0.8 µm with a differential mobility analyzer. Mass size distributions in the aerodynamic size range of 0.032–17 µm were determined with an 11-stage Berner-type, low-pressure impactor. For particles larger than 3 µm, a precyclone, wind-sieve method was applied.

The gas composition was measured after the electrostatic precipitator. The particle size distributions were measured from samples taken at the flue gas fan at the boiler exit before the electrostatic precipitator, when the sootblowers were turned off. We have modeled the boiler on the circumstances prevailing during these measurements.

	DEPOSITS		FUME	
Element	Base case	Low sulfur	Base case	Low sulfur
Na, %	23	21	30	26
K, %	4	20	3	0
Cl, %	0	30	0	4
S, %	17	3	19	7
C, %	0	2	0	6
O, %	35	16	39	35
Mech.,* %	21	8	13	14
Totals, %	100	100	100	100

*Mechanically produced particles.

II. Composition of fume (aerosol particles) and fume deposits in the second superheater

Element	Deposits	Fume
Na, %	33	33
K, %	3	3
Cl, %	9	8
S, %	6	6
C, %	5	5
O, %	32	31
Mech.,* %	12	18
Totals, %	100	100

*Mechanically produced particles.

III. Composition of fume and fume deposits in the first economizer

Model input

Inputs for the model included the boiler geometry, the temperatures for the flue gas and heat transfer surface at different locations, the amounts of elements volatilized from black liquor, and the amount of air injected. The boiler was simulated beginning at the level at which black liquor is injected and ending after the electrostatic precipitator. Figure 2 presents the scheme, showing cross sections of the various areas.

We assumed that the elements were volatilized, in given fractions, at the start of the simulation. The simulation was started at the maximum temperature of 1600°C, and the gases were assumed to cool to 1300°C in 1 m, as in the simulation of Wessel and co-workers *(9)*. Results are not sensitive to the maximum gas temperature, as long as it is above the condensation temperature of sodium sulfate, which in the base case is 1370°C. Other gas temperature values were obtained from a boiler manufacturing company.

Estimates for the heat transfer surface temperatures were calculated on the basis of gas and steam temperatures and melting points of the deposited layer *(21)*. We used temperature differences of 200°C, 100°C, 75°C, and 50°C for Superheaters 1–4, respectively. For the first, second, and third boiler banks, we used differences of 100°C, 75°C, and 50°C, respectively. From the first economizer to the second economizer, the difference was set to 100°C. For the rest of the boiler, the difference was set to 50°C.

There are no direct data on the volatilized fractions in recovery boiler conditions. Consequently, the amounts of the volatilized elements were set to correspond roughly with the gas composition measured after the electrostatic precipitator and in keeping with the boiler mass balance.

We postulated that metal oxides provide the seed particles for the condensation of the gaseous sodium and potassium sulfates. Their input size distribution was given as a log-normal distribution with a number median diameter of 60 nm. According to our model, the primary particles do not grow as large as the coarse particles, which range from 2 µm to 20 µm *(2)*. According to the measurements, the chemical composition of the coarse particles does not differ much from that of the smaller particles. Currently, it is not known how these coarse particles are formed. We simply add a mode of inert particles with an initial log-normal size distribution, which has a mass median diameter at 5 µm, and call them "mechanically produced" particles. The idea here is to study their deposition behavior as they are transported through the boiler. In the simulations, we have kept the amount of coarse particles below the value measured before the electrostatic precipitator.

Two cases with different black liquor compositions were calculated for the boiler. Table I lists results for a base case and a case with low sulfur. In the base case, we used the fuel elemental analysis of the black liquor (67% dry solids) that was being fired during the measurements.

In the case of low sulfur, we simulated aerosol dynamics in the same boiler as though it were burning a black liquor that had a higher chlorine content and a lower sulfur content than the base-case liquor. In addition, volatilization ratios for these species were changed. The injection rates of all other components were kept the same as in the base case which resulted in a slight decrease in the total injection rate. The purpose was to demonstrate the role of sulfur and chlorine in black liquor combustion.

In the ABC model, we simulated the black liquor as being injected at a rate of 28.2 kg/s in the base case and 27.4 kg/s in the case of low sul-

fur. Primary and secondary air were injected at 64.0 kg/s (88%), and tertiary air was injected at 7.7 kg/s (12%).

Gas-phase chemistry and particle formation

Sodium sulfate starts to condense at 1370°C in the base case and at 1310°C in the case of low sulfur. These temperatures occur during the rapid cooling in the first simulated meter. In the base case, the condensation of sodium sulfate depletes nearly all of the gas-phase sodium. Potassium sulfate begins to condense at 1180°C.

In the case of low sulfur, it is the amount of gas-phase sulfur that limits the formation of condensed sodium sulfate. The rest of the available sodium reacts with carbon to produce condensed sodium carbonate, starting at 1120°C according to the equilibrium. Sodium and potassium chlorides remain in the gas phase at this stage and condense later in the superheater section, starting at 790°C and 740°C, respectively.

In the case of low sulfur; three successive steps can be detected in Fig. 3 as increases in particle concentration. The first step occurs immediately, as sodium sulfate condenses in the first meter. The second increase is for sodium carbonate, which reaches its highest point just before the tertiary air. The third increase occurs with the formation of sodium and potassium chloride at about 35 m. The graphs in Fig. 4 present the species concentrations and compositions of gaseous sodium (upper graphs) and potassium (lower graphs). These graphs highlight the fact that the use of low-sulfur liquors can lead to high concentrations of gaseous alkali chlorides in the superheater section, which makes possible the phenomenon of vapor depostion on heat exchanger tubes.

Particle size distribution and chemical composition

The graphs in Fig. 5 present particle mass size distributions and chemical compositions before the injection of tertiary air (upper graphs) and before the electrostatic precipitator (lower graphs). The total area in these figures is proportional to the total normalized (0°C) mass concentration. Each shaded area is proportional to the normalized mass concentration of the respective species.

In the base case, the mass size distribution peaks at 0.7 µm, which is reached before the injection of tertiary air and which essentially remains the same. A small part of the sulfates have condensed on the mechanically produced particles. The peak in potassium sulfate concentration is at a slightly larger particle size than the peak in sodium sulfate concentration. Because agglomeration is insignificant at low number concentrations when there are no particles smaller than 0.1 µm, after the injection of tertiary air the mass size distribution is changed only by deposition on external surfaces. The normalized particle concentration is decreased by more than half as the particles are transported through the boiler to the electrostatic precipitator.

In the low-sulfur case, the mass size distribution peak is broader. The particle concentration attains its maximum value in the superheater section, when sodium and potassium chlorides have condensed. Sodium sulfate, which is the first to condense, is enriched in smaller particles. The chlorides, which are the last to condense, are enriched in larger fume particles (lower right).

The simulated mass size distribution is in qualitative accordance with the measured distribution (lower left), assuming that particles are spherical and have a density of 2500 kg/m^3. The normalized total mass concentrations are quite similar, and the calculated chemical composition is in accordance with the measured chemical composition. Some fume particles seem to grow larger than predicted.

The agreement between the number size distributions is good, as Fig. 6 shows. Nevertheless, the peak in the simulated number size distribution before the electrostatic precipitator (0.5 µm) is at a slightly larger particle size than in the measured one (0.3 µm). The simulated total number of particles is also above the measured value.

At this stage of modeling, the simulation results are in satisfactory accordance with the measured results, at least with respect to the fume formation model. The difference in mass size distribution is probably associated with fume transport in the flue gas channel. The difference could result from re-entrainment of particles or from the effects of sootblowing before the economizers. The number size distribution is not so much affected by fume transport, so the measured number size distribution gives a better indication of the primary particle formation. Discrepancies can arise from nonhomogeneous turbulent conditions or from errors in the estimates of volatilized fractions or seed size distribution. The only size distribution measurements available were made before the electrostatic precipitator. Therefore, we cannot properly distinguish between inaccuracies in the fume formation model and inaccuracies in the description of fume transport.

Deposition

Deposition layer growth rates are calculated on the assumption that all particles stick when they deposit on external surfaces. Figure 7 charts deposition layer growth rates through the boiler. For comparison with the measured results, this approximation is quite good, since

KEYWORDS
Aerosols, alkali metals, alkalis, colloids, cooking liquors, deposition, dispersions, dynamics, fouling, fumes, furnaces, heat exchangers, kraft liquors, mathematical models, mechanics, models, recovery furnaces, sodium, sols.

the sootblowing was turned off at the economizers during the measurements. In the bends, though, reentrainment can be significant even under these conditions. According to our results, most of the deposition can be attributed to thermophoresis. The geometry of the heat transfer surfaces and its effect on deposition were not considered in detail in these calculations.

The only qualitative difference between the base case and the low-sulfur case is that vapor deposition of sodium and potassium chloride on superheater surfaces is important in the low-sulfur case. Vapor deposition is more important than particle deposition in the first superheater, as Fig. 8 illustrates. Deposited chloride vapors also serve as a kind of a glue by decreasing the melting point of the deposited layer and making heat exchanger surfaces sticky for particles to deposit further into the superheater section.

Deposition velocities at different locations in the boiler have been computed on the basis of the flow conditions, as presented in Fig. 9. Deposition velocities in the bends seem to be high, regardless of particle size. For deposition in the first economizer, there is a minimum for 3-µm particles. Particles smaller than 3 µm are mainly deposited by thermophoresis, and particles larger than 3 µm are deposited primarily by turbulent impaction. The steep rise in the deposition velocity above 10 µm explains why the mechanically produced particles with a diameter larger than 10 µm (Fig. 5, upper graphs) are no longer entrained in the gas before the electrostatic precipitator (Fig. 5, lower graphs). For the second superheater, the model predicts a minimum deposition velocity for 10-µm particles.

The average elemental composition of the deposited fume particles is much the same as that of the gas-phase fume particles. The composition of the deposited layer is affected by carryover and vapor deposition, of which only vapor deposition is currently incorporated in the model. In Table II, note the high fractions of chlorine and potassium in the second superheater deposits that arise from vapor deposition in the low-sulfur case. (These percentages are 20% for Cl and 30% for K, as opposed to 4% and 0% in the base case.)

The differences in composition, when only particle deposition occurs, arise from different deposition velocities for different particle sizes. For instance, the largest particles, those that are mechanically produced, have the highest deposition rate; therefore, they become enriched in the deposition layers.

Table III presents fractions for the fume and fume deposits in the first economizer. In the low-sulfur case, the fraction of chlorine in the deposited layer in the first economizer is 11% smaller than the chlorine content of the gas-phase fume particles (8% vs. 9%). On the other hand, the fractions of sulfur are nearly the same (6%). Compared with sulfur, chlorine is concentrated in larger fume particles, or in particle sizes nearer to the deposition rate minimum.

CONCLUSIONS

We have developed a computer model for fume formation and deposition in kraft recovery boilers. This model, the ABC model, is based on the numerical simulation of aerosol dynamics *(1)*. Gas-phase chemical reactions of alkali species, fume formation by vapor condensation, fume particle growth by condensation, and agglomeration are included in the program, along with a detailed description of fume deposition.

As an example case, we have calculated alkali salt fume deposition in a boiler where we have carried out detailed characterization studies on fume particles *(2–5)*. Calculated results have been presented for the black liquor used in the boiler during the characterization studies as well as for a low-sulfur liquor. The calculated fume particle size distributions and chemical compositions have been compared with experimental results.

In the future, we hope to validate the fume formation model with measurements made at the furnace exit. The deposition model needs to be validated as well before it can be used for quantitative predictions of fume deposition in recovery boilers. While we will continue to try to make the results more accurate, the results already obtained give us insights on the parameters that affect fume deposition. The model can predict the composition and the growth rate of the deposition layer on the basis of black liquor composition and operating conditions. TJ

Jokiniemi is group manager with VTT Energy, Aerosol Technology Group. Pyykönen is a research scientist in the same group. Kauppinen is group manager with VTT Chemical Technology, Aerosol Technology Group. Mikkanen is a research scientist in the same group. The address for all authors is P.O. Box 1401, FIN-02044 VTT, Finland.

This study is a part of the Finnish combustion research program LIEKKI and is funded by the Finnish Ministry of Trade and Industry and the companies Ahlström Corp. and Tampella Power. In addition, the authors want to thank Veitsiluoto Oulu mills, Metsä-Botnia Kemi mills, Kauko Janka, Esa Vakkilainen, and Pekka Siiskonen for their technical support.

Received for review June 3, 1995.

Accepted Nov. 17, 1995.

LITERATURE CITED

1. Jokiniemi, J. K., Lazaridis, M., Lehtinen, K.E.J., *et al., J. Aerosol Sci.* 25: 429(1994).
2. Mikkanen, P., Kauppinen, E. I., Jokiniemi, J. K., *et al.*, *The 1993 Forest Products Symposium Notes*, AIChE Symposium Series 90, Am. Inst. Chem. Engineers, New York, pp. 46–54.
3. Mikkanen, P., Kauppinen, E. I., and Jokiniemi, J. K., "The Effect of Black Liquor Characteristics on Alkali Salt Aerosols in Industrial Recovery Boilers," paper presented at the Thirty Years Recovery Boiler Co-operation in Finland, Intl. Conf., May 24, 1994.
4. Mikkanen, P., Kauppinen, E. I., Jokiniemi, J. K., *et al.*, *Tappi J.* 77(12): 81(1994).
5. Mikkanen, P., Kauppinen, E. I., Jokiniemi, J. K., *et al.*, "Characteristics of Aerosols from Industrial Scale Black Liquor Combustion," to be submitted for publication in *J. Aerosol Sci.*
6. Friedlander, S. K., *Smoke Dust and Haze*, John Wiley, New York, 1977.
7. Kauppinen, E. I., Mikkanen, M. P., Valmari, T., *et al.*, *TAPPI 1995 International Chemical Recovery Conference Proceedings*, TAPPI PRESS, Atlanta, p. B105.
8. Pejryd, L. and Hupa, M., *TAPPI 1984 Pulping Conference Proceedings*, TAPPI PRESS, Atlanta, p. 579.
9. Wessel, R. K., Parker, K. L., and Akan-Etuk, A., *TAPPI 1993 Engineering Conference Proceedings*, TAPPI PRESS, Atlanta.
10. Srinivasachar, S., Helble, J. J., Ham, D. O., *et al.*, *Prog. Energy Combust. Sci.* 16: 303(1990).
11. Steinberg, M. and Schofield, K., *Prog. Energy Combust. Sci.* 16: 311(1990).
12. Wessel, R. K., Parker, K. L., and Verril, C. L., *TAPPI 1995 Engineering Conference Proceedings*, TAPPI PRESS, Atlanta.
13. Helble, J., Neville, M., and Sarofim, A. F., 21st International Symposium on Combustion, 1986, p. 411.
14. Hinze, J. O., *Turbulence*, McGraw Hill, New York, 1975, Ch. 5.
15. Im, K.H. and Chung, P. M., *AIChE J.* 29(3): 498(1983).
16. Talbot, L., Cheng, R. K., Schefer, R. W., *et al.*, *J. Fluid Mech.* 101(4): 737(1980).
17. Friedlander, S. K. and Johnstone, H. F., *Ind. Eng. Chem.* 49: 1151(1957).
18. Israel, R. and Rosner, D. E., *Aerosol Sci. and Tech.* 2: 45(1983).
19. Levenspiel, O., *Chemical Reaction Engineering*, 2nd edn., John Wiley, New York, 1972.
20. Jokiniemi, J. K., Pyykönen, J., Lyyränen, J., *et al.*, to be published in *1995 Conference Proceedings, "Application of Advanced Technology to Ash-Related Problems in Boilers,"* Engineering Foundation.
21. Tran, H. N., *Tappi J.* 69(11): 102(1986).

EQUATIONS

$$\frac{d\left(\rho_{dk} Y_{jk}\right)}{dx} = \left[\frac{d\left(\rho_{dk} Y_{jk}\right)}{dx}\right]_{gtp} + \left[\frac{d\left(\rho_{dk} Y_{jk}\right)}{dx}\right]_{agg} - \frac{V_{dk} A_d}{u \Delta V} \rho_{dk} Y_{jk} \qquad (1)$$

$$\frac{dc_j}{dx} = \left(\frac{dc_j}{dx}\right)_{form} - \left(\frac{dc_j}{dx}\right)_{gtp} - \frac{V_{dk} A_d}{u_g \Delta V} c_j \qquad (2)$$

$$V_d = \frac{J_p}{n(x)} = \frac{1}{\left(1/v_f\right) + \left(1/v\right)} \qquad (9)$$